Materials Research. 2020; 23(4): e20200013
DOI: https://doi.org/10.1590/1980-5373-MR-2020-0013

Experimental Investigation of the Sawn Surface of Monocrystalline Silicon Cut by Endless Diamond Wire Sawing

Erick Cardoso Costa*[a] , ***Caroline Piesanti dos Santos*[a]**, ***Fabio Antonio Xavier*[a]**,

***Walter Lindolfo Weingaertner*[a]**

[a]*Universidade Federal de Santa Catarina (UFSC), Departamento de Engenharia Mecânica, Laboratório de Mecânica de Precisão (LMP), CEP 88040-900, Florianópolis, SC, Brasil*

Received: January 13, 2020; Revised: May 1, 2020; Accepted: July 9, 2020

The aim of this study was to investigate the influence of the cutting parameters on monocrystalline silicon cut by diamond wire sawing. The sawn surface was analyzed in terms of surface morphology, surface roughness, material removal mechanism and residual stress (by Raman spectroscopy). The surface morphology exhibited evidence of both material removal mechanisms: the brittle mode and the ductile mode. The surface roughness increased with a high v_f, which promoted the formation of craters on the sawn surface. On applying a higher v_c, the surface roughness reduced, since this favored the formation of damage-free grooves. The Raman spectrum showed evidence of different residual crystalline phases on the sawn surface, which confirms the material removal mechanisms. An increase in v_f, for the same v_c, caused at reduction in the compressive stress, since the brittle mode predominated as the material removal mechanism. Maintaining v_f constant and increasing v_c results in higher compressive stress, caused by plastic deformation of the silicon during chip formation.

Keywords: *Diamond wire sawing, Monocrystalline silicon, Brittle-to-ductile transition, Residual stress, Phase transformation*

1. Introduction

Solar energy generation using photovoltaic energy systems is one of the main renewable power sources due to its high efficiency and low greenhouse gas emissions[1]. However, many factors restrict the dissemination of this technology, in particular, the costs associated with the materials required and the machining operations (representing 30-40% and 50% of the total solar cell manufacturing cost, respectively)[2]. Crystalline silicon (c-Si) is the main material used for solar cell manufacturing, representing around 80% of solar cells manufactured worldwide to date. Its dominance in this sector is mainly due to two factors: the abundance of Si in the Earth's crust (accounting for 27% of all minerals) and its semiconductor characteristic[3].

Despite its advantages, c-Si presents low fracture toughness, which makes it difficult to machine. In the photovoltaic industry, multi-wire sawing (MWS) is currently the primary machining process. As shown in Figure 1a, MWS is based on a single wire fed from a supply-spool to a take-up spool, creating a web with parallel and equidistant wires that are guided by grooved rollers. Prior to the MWS process, c-Si ingots, with a diameter up to 300 mm, are produced. In essence, the wire web is pulled by the torque applied in the main drive pulley, while the c-Si ingot is pushed against the wire web, resulting in wafers with thickness between 100 and 180 μm[4].

Two different forms of material removal mechanism can carry out the MWS process: multi-wire slurry sawing (MWSS) or multi-diamond wire sawing (MDWS). In the former (Figure 1b), the cut is performed using an abrasive slurry based on polyethylene glycol with silicon carbide (SiC) grains, which flows through nozzles onto the wire and is then taken into the cutting channel. Interaction between the SiC grains and the c-Si substrate results in material removal by three-body wear. On the other hand, in MDWS, diamond abrasives electroplated with nickel on steel wire are used. As seen in Figure 1c, the cut is performed by two-body wear, involving direct interaction between the diamond grains and the c-Si substrate[4,5].

Both of these MWS processes are stable along the production chain, but MDWS has advantages over MWSS, including a higher material removal rate, lower surface and subsurface damage, and the use of a water-based coolant. Nevertheless, the adverse effects on the surface integrity of the c-Si wafer, such as surface roughness, micro-cracks in the surface and subsurface, and phase transformation, are still unavoidable[6]. In this regard, a high degree of process control is required during machining, since the cutting quality and performance are dependent on the cutting process parameters.

In this context, the MWS kinematics, brittleness of the c-Si and reciprocating movement hinder the experimental investigation of the influence of the cutting process parameters[5,7]. Therefore, optimization of the cutting process is dependent on empirical knowledge, based mainly on the operators' experience and a trial and error approach[8]. To reduce the solar cell manufacturing costs and make solar energy more viable, it is necessary to understand the different stages that make up the production chain, including the diamond wire sawing process[9]. Thus, an experimental approach was applied using an endless wire saw test rig to investigate monocrystalline

*e-mail: erick.cardoso.costa@posgrad.ufsc.br

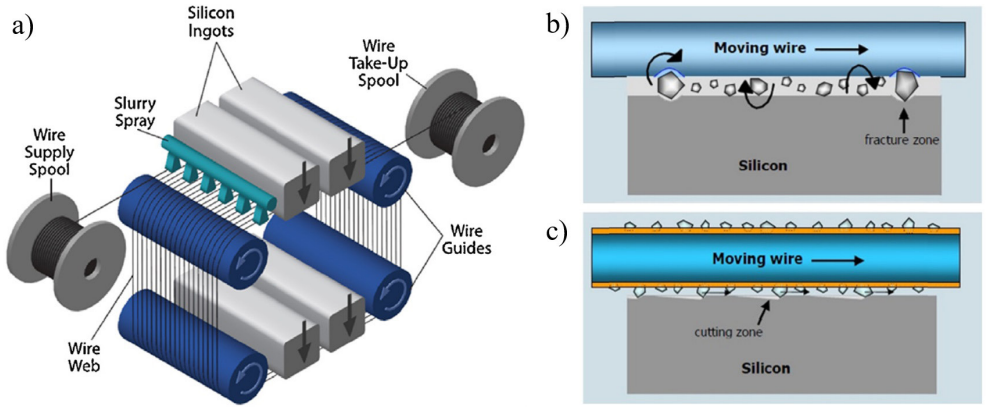

Figure 1. Multi-wire sawing process: a) machine-tool; b) multi-wire slurry sawing; c) multi-diamond wire sawing (adapted from Wu[5]).

silicon (mono-Si) cutting employing the diamond wire sawing process. The sawn surface was evaluated in terms of surface morphology, surface roughness and phase transformation, varying the wire cutting speed (v_c) and feed rate (v_f), and the results are reported herein.

2. Materials and Methods

2.1. Machine-tool

Experiments were performed on an endless wire saw test rig designed by Knoblauch[10] with an ultra-precision machining system built by Stoeterau[11], as shown in Figure 2. The test rig is based on aerostatic bearing technology, which ensures low friction on the bearings and guides. A looped diamond wire, wrapped in Teflon pulleys (A and A'-axis), executes the cut through a continuous wire cutting movement. A three-phase electric motor powers the A-axis and a control panel with a frequency inverter sets the wire cutting speed (up to v_c = 26 m/s). Vertical aerostatic bearings (Y-axis) push the workpiece against the wire with a minimum feed rate of v_f = 0.08 mm/min. The wire tension (T_{wire}) is regulated by the air pressure control of a pneumatic cylinder (X-axis), while wafer thickness is adjusted through a screw (Z-axis).

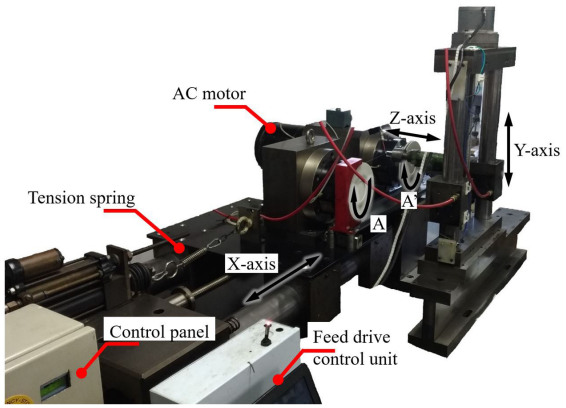

Figure 2. Endless wire saw test rig.

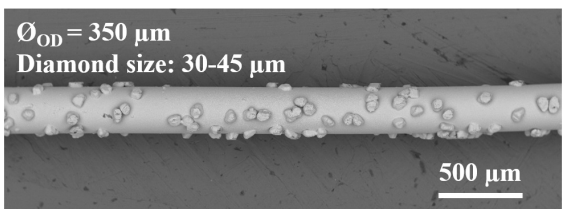

Figure 3. SEM of the Ni-electroplated diamond wire.

2.2. Cutting tool and workpiece

An Ni-electroplated diamond wire with outer diameter of $Ø_{OD}$ = 350 µm and diamond size of 30-45 µm was used as the cutting tool (see Figure 3). Industrial machine tools use around 5-10 km of diamond wire to cut the c-Si ingots. For this investigation, both butts of a short-length diamond wire (1 ± 0.05 meters) were welded using a resistance welding device developed by Souza[12]. The advantage of employing a looped diamond wire is that cuts are performed with a constant wire cutting speed.

Solar-grade mono-Si blocks with dimensions of 50 mm x 7 mm x 25 mm, as shown in Figure 4a, were used for the cutting experiments. Mono-Si specimens were cut with a thickness of 1±0.05 mm in the crystallographic orientation (100), since this orientation is widely employed in solar cell manufacturing, and the crystallographic orientation (010) was orthogonal to the wire cutting movement. The Figure 4a show the dimensions of the mono-Si workpiece and the Figure 4b show the crystallographic orientation of the mono-Si in function of the wire cutting direction.

2.3. Experimental procedure

In order to evaluate the sawn surface of the mono-Si cut using the diamond wire sawing process, the cutting parameters wire cutting speed (v_c) and feed rate (v_f) were varied and each parameter had three levels (low, medium and high). During the cutting experiments, the wire tension was kept constant at 30 N and all tests were performed without cutting fluid. For each cutting experiment, a new (unused) Ni-electroplated diamond wire was used, to avoid the tool wear effect. Table 1 summarizes the cutting conditions employed in this study.

The kinematics involved in the cutting process consisted of subjecting the mono-Si specimens to a vertical movement

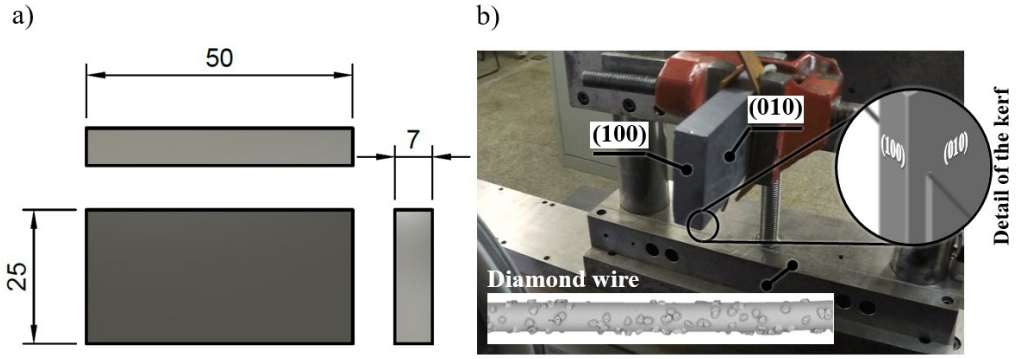

Figure 4. Mono-Si workpiece: a) dimensions (mm); b) crystallographic orientation in function of the wire cutting direction.

with constant feed rate (v_f) against the single-diamond wire, which has a constant wire cutting speed (v_c). Figure 5 shows the kinematics of the cutting experiments.

A full factorial design of experiments (DoE) was generated, resulting in 9 tests. Each cutting condition was applied three times. Analysis of variance (ANOVA), with Statistica 13® software, was used to compare the average surface roughness values obtained. The significance of the effect of variables (v_c and v_f) was determined considering a confidence interval of 95% and significance level of 5%.

2.4. Surface analysis methods

2.4.1. Surface morphology

The surface morphology under different cutting conditions was characterized through scanning electron microscopy (SEM) on a Hitachi TM-3030 microscope. This allowed the observation of the main material removal mechanisms (ductile and brittle mode) when mono-Si is cut applying the diamond wire sawing process.

2.4.2. Surface roughness

The surface roughness of the sawn mono-Si specimens was measured using a contact profilometer (Taylor Hobson, FTS i-120). Table 2 shows the stylus dimensions and additional measuring parameters. The measuring conditions adopted adhere to the ISO 4288 standard[13] and the standard cut-off (λ_c) value was 0.8 mm.

With the above-mentioned measurement setup, the profiles of the sawn mono-Si specimens were measured three times, perpendicularly to the cutting direction. The MountainsMap Universal 7.1 software program was used to process the measured data according to the recommendations of the ISO 4287 standard[14]. The surface roughness parameters evaluated were the arithmetical mean deviation (R_a) and total height (R_z). The values correspond to the arithmetic mean and the respective standard deviation.

2.4.3. Phase transformation

The occurrence of phase transformation on the sawn surface of the mono-Si specimens induced by the diamond wire sawing process was investigated using Raman spectroscopy analysis (Renishaw inVia micro-Raman microscope with Ar-laser, $\lambda = 514.2$ nm). Raman spectra were obtained from three data acquisition runs (each of approximately 30s) in the spectral range of 200 to 700 cm^{-1}. The Ar-laser was focused on two different regions of the mono-Si specimens to identify residual crystalline structures present on the sawn surface.

Firstly, the aim was to characterize the material removal mechanism (ductile and brittle mode) by identifying the crystalline phases observed on the Raman spectra. A procedure proposed by Weinstein and Piermarini[15] was then employed to estimate the residual stress values. The spectrum for the

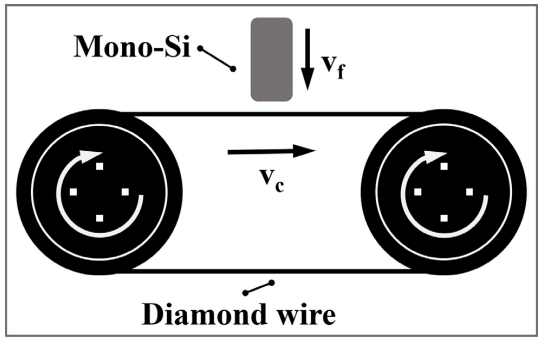

Figure 5. Kinematics of the cutting process.

Table 1 – Cutting conditions applied in the experiments.

Parameters	Cutting condition			Unit
Wire cutting speed (v_c)	10	15	20	m/s
Feed rate (v_f)	20	30	40	mm/min
Wire tension		30		N
Cutting fluid		none		-

Table 2 – Setup for surface roughness measurements of sawn mono-Si specimens.

Measurement parameter	Characteristic
Stylus	Diamond
Stylus tip radius (r_{stylus})	2 µm
Stylus cone angle	90°
Transverse length (l_t)	5.6 mm
Evaluation length (l_n)	4 mm
Cut-off (λ_c)	0.8 mm

diamond cubic structure (Si-I phase), with a value of 521 cm^{-1}, was used as a reference (ω_o) and this value was applied in Equation 1 to estimate the residual stress.

$$\omega = \omega_o + 0.52*P \quad (1)$$

where ω (cm^{-1}) is the spectral value for the Si-I phase, ω_o (cm^{-1}) is the reference spectral value for the Si-I phase and P is the estimated residual stress (kbar).

3. Results and Discussion

3.1. Surface morphology analysis

The surface morphology of sawn mono-Si specimens under different cutting conditions is shown in Figure 6. It can be observed that the sawn surface presents regions that underwent material removal in the brittle and ductile modes, with the presence of craters/pitting and damage-free grooves, respectively. According to Liu et al.[16], craters and pitting are formed due to the brittleness of silicon and can be explained by the fracture mechanics theory, as reported by Möller[4]. Moreover, Klocke[8] states that crater formation is the result of a higher undeformed chip thickness (h_{cu}). Bifano et al.[17] reported that there is a threshold ($h_{cu.crit}$) between plastic deformation and micro-crack formation in the machining of brittle materials. At the highest penetration depth the critical limit ($h_{cu,crit}$) is exceeded, leading to chip formation via micro-crack propagation, and the ductile machining of these materials cannot be achieved. This behavior is observed in Figure 6a and 6b, when v_f increases from 20 to 40 mm/min, with same v_c value. An increase in v_f leads to the $h_{cu} > h_{cu,crit}$ condition, which results in a sawn surface with wider and deeper craters.

On the other hand, an increase in v_c from 10 to 20 m/s induces a predominance of the ductile mode and the presence of more damage-free grooves, as seen in Figure 6c and 6d. Parallel and oriented grooves follow the cutting direction, being produced by the restricted orientation of the diamond grains on the steel wire[3]. These damage-free grooves are formed through the ductile material removal mechanism, caused by an increase in v_c, which consequently decreases the h_{cu} value. Under the $h_{cu} \leq h_{cu,crit}$ condition, chip formation occurs by plastic deformation, since the silicon does not reach its fracture toughness limit. Figure 6c and 6d show that an increase in v_c results in a sawn surface with little evidence of brittle fracture and more ductile regions.

Thus, the predominance of the ductile or brittle mode is dependent on the cutting conditions employed. In this case, a lower v_f along with a higher v_c generated the predominance of the ductile mode on the sawn surface of mono-Si.

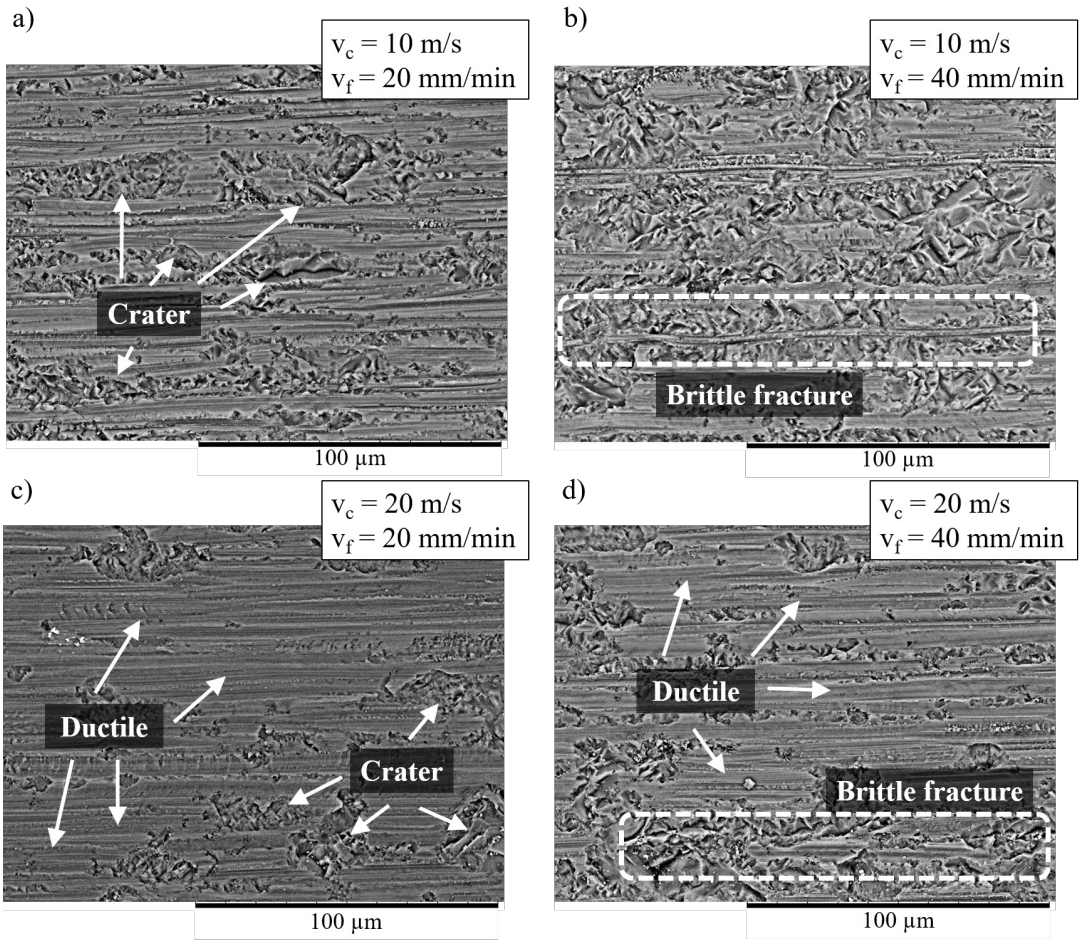

Figure 6. Morphology of sawn surface of mono-Si specimens cut under different cutting conditions.

3.2. Surface roughness analysis

Figure 7 shows the average values for surface roughness parameters R_a and R_z under different cutting conditions. An increase in the average values can be observed for both surface roughness parameters with a high v_f for the same v_c. According to Klocke[8], an increase in v_f results in a greater penetration depth of the diamond grain, leading to surface formation in the brittle mode. Thus, the sawn surface presents deeper craters, increasing the surface roughness (R_a and R_z).

On the other hand, for a constant v_f, an increase in v_c caused a reduction in both surface roughness parameters (R_a and R_z). Bifano et al.[17] reported that this result is produced by a higher engagement frequency of the kinematics cutting edges when the v_c increases, lowering the h_{cu} and leading to a surface formed predominantly in the ductile mode. Therefore, the sawn surface presents more regions with damage-free grooves, decreasing the surface roughness, as seen in Figure 7.

The behavior of the surface roughness parameter R_a is attributed to the predominance of the brittle or ductile mode on the sawn surface of the mono-Si specimen[18]. In comparison with surface morphology observed in Figure 6b, the sawn surface presents larger and wider craters, which indicates the predominance of the brittle cutting mode. Based on the wide distribution of peak-and-valley, the arithmetical deviation mean was affected, since R_a exhibited higher average value. In contrast, a reduction in R_a was observed when the mono-Si presented higher ductility during the surface formation. In the SEM micrograph in Figure 6c, the smooth aspect of the sawn surface is characterized by the presence of damage-free grooves generated from the microcutting and ploughing produced by the penetration of diamond grain into the workpiece, since the cutting conditions do not favor the fragile fracture mode ($h_{cu} \leq h_{cu,crit}$). As a result, the parameter R_a decreased due to a predominance of the ductile aspect of the sawn surface.

Another aspect of the surface morphology can be described by parameter R_z. According to Li et al.[19], this surface roughness parameter can be considered as the main topographic characteristic that expresses an equivalent value of h_{cu}. However, due to the multiple inhomogeneous contact of the diamond grains into the surface, the R_z value represents the highest h_{cu} assumed by a single diamond grain[6]. It can be assumed that different crater depths are produced with the variations in the cutting parameters. Thus, on keeping the same v_c, an increase in v_f would produce deeper craters, leading to a significant increase in the R_z value, which indicate an increase in h_{cu} with a variation in v_f. On the other hand, a reduction in the parameter R_z is attributed to a higher v_c value for same value of v_f. Due to higher engagement frequency of the diamond grain on workpiece surface, the h_{cu} of the active diamond grains decreases, resulting in less fragile fracture in the form of craters.

The behavior of both surface roughness parameters are in accordance with SEM micrographs of surface morphology of the mono-Si specimen. It was performed an ANOVA analysis to quantify the effect of the cutting parameters on surface roughness. Table 3 shows the ANOVA results for the surface roughness (R_a and R_z) of the sawn mono-Si specimens.

According to ANOVA, the *p*-values for the feed rate (v_f) and wire cutting speed (v_c) were 0.00570 and 0.02398, respectively, which indicates that both process parameters have a significant effect on the values of surface roughness parameter R_a. A higher feed rate (v_f) resulted in an increase of 21.0% in the R_a parameter. On the other hand, an increase in the wire cutting speed (v_c) resulted in a reduction of around 14.5% in the R_a parameter.

For the parameter R_z, the *p*-values for the feed rate (v_f) and wire cutting speed (v_c) were 0.00004 and 0.00015, respectively, demonstrating that both process parameters also have a significant effect on surface roughness parameter R_z. An increase in the feed rate (v_f) increased R_z by 27.9%, while on increasing the wire cutting speed (v_c) R_z decreased by around 20.2%.

3.3. Phase transformation

Raman spectroscopy was applied to examine the residual crystalline structures on the sawn surface. These structures can confirm the hypothesis of the material removal mechanism

Table 3. ANOVA results for surface roughness parameters (R_a and R_z).

Process parameter	Surface roughness	Mean effect (μm)	Percentage (%)	*p*-value
Feed rate (v_f)	R_a	+ 0.086	+ 21.0%	0.00570
Wire cutting speed (v_c)		− 0.070	− 14.5%	0.02398
Feed rate (v_f)	R_z	+ 1.312	+ 27.9%	0.00004
Wire cutting speed (v_c)		− 1.218	− 20.2%	0.00015

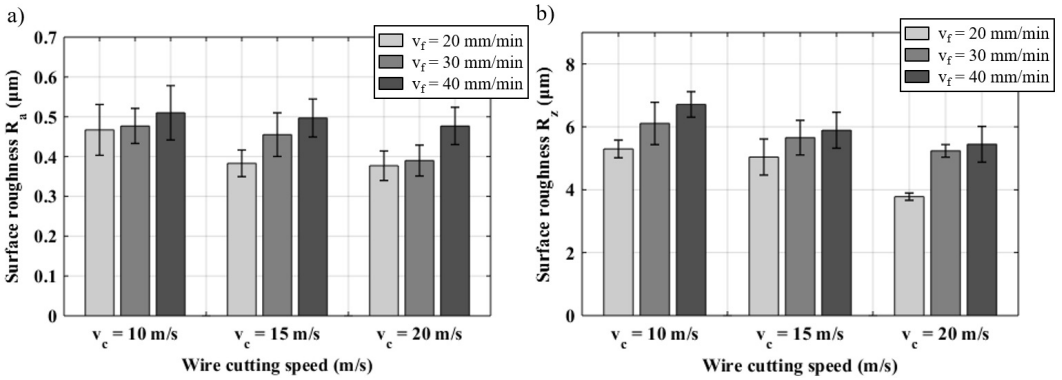

Figure 7. Surface roughness of sawn mono-Si specimens under different cutting conditions: a) R_a parameter and b) R_z parameter.

associated with mono-Si cutting using the diamond wire sawing process. The Raman spectra results for mono-Si sawn under the cutting condition of $v_c = 20$ m/s and $v_f = 20$ mm/min can be seen in Figure 8.

Initially, the Ar-laser was focused on the craters presents in sawn surface, resulting in a single peak at 521 cm^{-1}, corresponding to the diamond cubic structure (Si-I phase), as shown in Figure 8a. According to Suzuki et al.[20], the presence of single peaks indicates that the brittle mode dominated as the main material removal mechanism. This characteristic suggests that h_{cu} exceeded the critical limit ($h_{cu,crit}$) of the ductile-brittle transition, leading to chip formation through micro-crack propagation and the appearance of the pure crystalline silicon peak (Si-I phase).

The Ar-laser was then focused in the damage-free grooves and the Raman spectrum obtained is shown in Figure 8b. It can be observed that there is a peak at 525 cm^{-1} and a less intense band in the region of 425-510 cm^{-1} with peak at 469 cm^{-1}, associated with Si-I and a-Si phases (amorphous silicon), respectively. Bidiville et al.[21] reported that the presence of the a-Si phase is a consequence of the ductile behavior of mono-Si during chip formation and removal. According to Dominich and Gogotsi[22], this finding suggests that mono-Si underwent phase transformation due to high contact pressure ($\geq$ 12 GPa). The penetration of the diamond grain into the surface leads to mono-Si amorphization and when this occurs in conjunction with $h_{cu} \leq h_{cu,crit}$ the sawn surface will exhibit a less brittle fracture and the formation of more damage-free regions.

The Raman spectrum results are consistent with the surface morphology characteristics observed on the SEM micrographs. The sawn surface of the mono-Si specimens indicated a predominance of the brittle mode and a single Si-I peak was observed on the Raman spectrum. On the other hand, when damage-free grooves dominated, the Raman spectrum showed the presence of the band associated with the a-Si phase, which indicate that there was a plastic flow of the material on the rake face of the abrasive during the chip formation and removal. Other secondary crystalline phases of silicon were not detected on the sawn surface by Raman spectroscopy. The presence of only the a-Si phase on the sawn surface is attributed to the high wire cutting speed (v_c) used in this study.

3.4. Estimated residual stress

Figure 9 shows the Raman spectra obtained under different cutting conditions. It can be observed that there is a slight shift in the Si-I phase peak, considering a peak at 521 cm^{-1} as the reference. Furthermore, the intensity and bandwidth of the band associated with the a-Si phase also differ from the reference. According to Jasinevicius et al.[23], these findings indicate that the sawn surface is under residual stress. In order to estimate the residual stress of the sawn surface of the mono-Si specimens, Raman spectroscopy was employed applying the procedure proposed by Weinstein and Piermarini[15].

The residual stress results are reported in Figure 10. Considering the phase transformation characteristic of the silicon, the presence of secondary phases on the sawn surface suggests that the mono-Si underwent phase transformation from Si-I to Si-II during the cutting. According to Hertz's law for a tensile field, ductile behavior of brittle materials during loading occurs when the energy required to reach plastic deformation is lower than the micro-crack propagation energy. Under this condition, compressive stress predominates and the main material removal mechanism is the ductile cutting mode. Therefore, the residual stress of the sawn surface of the mono-Si specimen is compressive and the a-Si phase is observed as well as the shift in the Si-I phase peak.

As seen in Figure 10, a higher v_f, for same v_c, resulted in a decrease in the compressive stress on the sawn surface. Regarding the material removal mechanism, when v_f was varied from 20 to 40 mm/min, the surface morphology exhibited the brittle mode as the material removal mechanism predominant. The Raman spectra showed no secondary phases on the sawn surface, while the Si-I phase peak was slightly shifted.

An increase in the compressive stress values was noted for a higher v_c applying the same v_f. This is due to a higher engagement frequency of the diamond grains when v_c was increased, significantly decreasing the depth of cut and resulting in $h_{cu} \leq h_{cu,crit}$. Under this condition, phase transformation from Si-I to Si-II occurred, implying that the mono-Si was subjected to compressive stress during the penetration of the diamond grains and that chips were formed in the ductile mode. After the unloading of the diamond grain, the metastable phase (Si-II) changed to secondary

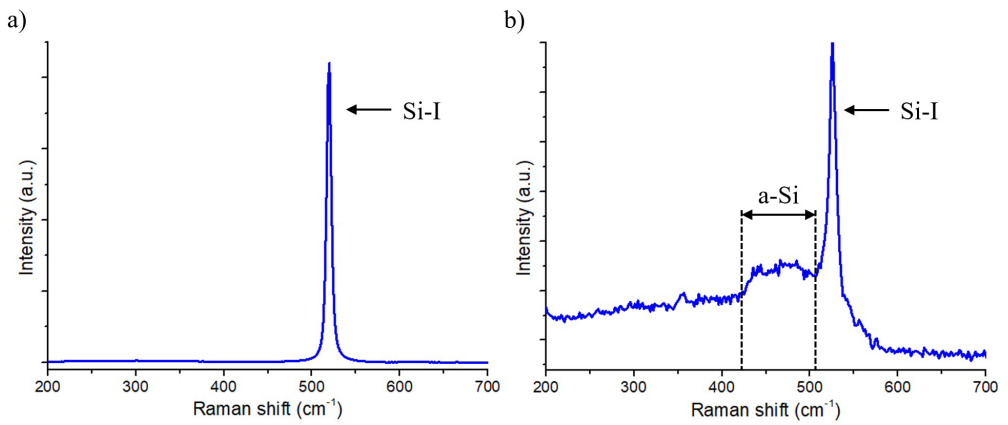

Figure 8. Phase transformation of sawn surface of mono-Si specimen.

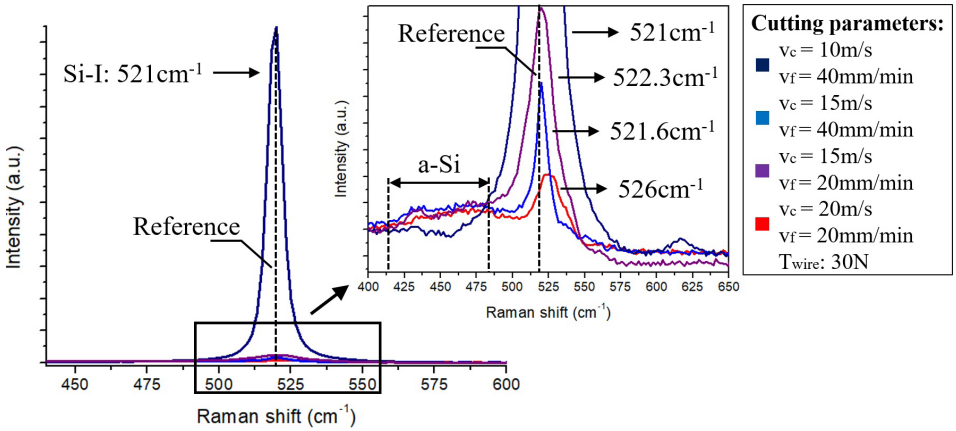

Figure 9. Displacement in the Si-I phase peak of the Raman spectra.

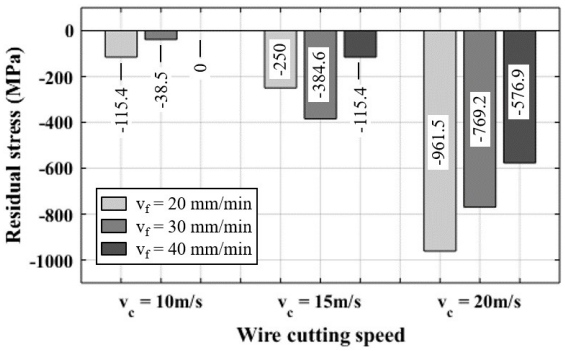

Figure 10. Estimated residual stress.

phases and, under faster unloading conditions, due to high v_c employed, the mono-Si surface presented the a-Si phase. In this regard, an increase in v_c led to material removal in the ductile mode, resulting in amorphization (a-Si phase) of the sawn surface of the mono-Si specimen and inducing higher residual compressive stress.

4. Conclusions

The influence of the cutting parameters wire cutting speed (v_c) and feed rate (v_f) on mono-Si specimens cut by endless diamond wire sawing was investigated. Both cutting parameters were found to have a significant effect on the sawn surface. Based on the results obtained from the experiments, it can be concluded that:

- The sawn surfaces of mono-Si specimens show evidence of different material removal mechanism when the cutting conditions (v_c and v_f) were varied. The brittle mode is predominant at higher v_f, leading to the presence of craters and pitting on the sawn surface. In contrast, increasing v_c resulted in better morphological aspects, with the formation of damage-free grooves.
- The surface roughness was analyzed in terms of the parameters R_a and R_z. The results showed that an increase in v_f resulted in surface characteristics formed through the brittle mode, which led to high values for the surface roughness. Increasing v_c resulted in a reduction of both surface roughness parameters, since the ductile mode dominated the formation of the sawn surface. It was observed that both surface roughness parameters (R_a and R_z) are influenced by predominance of material removal mode on sawn surface of mono-Si.
- The sawn surface of mono-Si specimens underwent phase transformation during the cutting. A single peak associated with the Si-I phase was observed on the Raman spectrum for the surface craters, which is in accordance with the brittle mode. The band attributed to the a-Si phase was detected on the spectrum for the damage-free grooves, which characterizes ductile regions.
- There was a slight shift in the Si-I phase peak on the Raman spectrum (in relation to the reference), indicating that the sawn surface was under residual stress. Thus, the residual stress values were estimated. According to the phase transformation characteristics of mono-Si, the presence of the a-Si phase indicates compressive stress. Regarding the cutting conditions, it was noted that increasing v_f reduces the residual stress due to the predominance of the brittle mode. The highest compressive stress was associated with the highest v_c, which indicates ductile behavior of the mono-Si during chip formation.

5. Acknowledgments

The authors would like to thank the Brazilian governmental agencies CAPES and CNPq for funding this research; Saint-Gobain Abrasives for supplying the electroplated diamond wire; the Swiss Federal Institute of Technology Zurich – ETH for providing the mono-Si blocks; and the Materials Laboratory (LabMat – UFSC).

6. Reference

1. Monteiro NSC, Monteiro RAB, Mariano JD, Junior JU, Romano CA. Brazil Market outlook for photovoltaic solar energy: a survey study. Br J Appl Sci Technol. 2017;21(5):1-11.

2. Peguiron J, Mueller R, Zanetti J, Habegger S, Burri M, Sopra FM. Reducing wire wear by mechanical optimization. Article PV Production Annual. Meyer Burger. 2014;1-9.
3. Yu X, Wang P, Li X, Yang D. Thin Czochralski silicon solar cells based on diamond wire sawing technology. Sol Energy Mater Sol Cells. 2012;98:337-42.
4. Möller HJ. Wafering of silicon. Semicond Semimet. 2015;92:63-109.
5. Wu H. Wire sawing technologies: state-of-the-art review. Precis Eng. 2016;43:1-9.
6. Costa EC, Santos CP, Xavier FA, Weingaertner WL. Influence of diamond wire sawing parameters on subsurface microcracks formation in monocrystalline silicon wafer. In: 25th International Congress of Mechanical Engineering; 2019 Oct 20-25; Uberlândia, MG, Brazil. Proceedings. Rio de Janeiro: ABCM. p. 1-8.
7. Bidiville A, Wasmer K, Van Der Meer M, Ballif C. Wire-sawing processes: parametrical study and modeling. Sol Energy Mater Sol Cells. 2015;132:392-402.
8. Klocke F. Manufacturing processes 2: grinding, honing, lapping. USA: Springer; 2009.
9. Costa EC, Souza RD, Knoblauch R, Weingaertner WL, Xavier FA, Wegener K. Corte de silício monocristalino com serra de fio diamantado contínuo. In: 10th Congresso Nacional de Engenharia Mecânica; 2018 May 20-24; Salvador, BA, Brazil. Proceedings. Rio de Janeiro: ABCM. p. 1-7.
10. Knoblauch R, Costa JVMT, Weingaertner WL, Xavier FA, Wegener K. Endless diamond wire saw for monocrystalline silicon cutting. In: 59th Ilmenau Scientific Colloquium. 2017 Sept 11-15; Ilmenau, Germany. Proceedings. Ilmenau: Technische Universität Ilmenau. p. 1-12.
11. Stoeterau RL. Desenvolvimento do protótipo de uma máquina-ferramenta comandada numericamente para usinagem de ultraprecisão com ferramenta de geometria definida [tese]. Florianópolis: Universidade Federal de Santa; 1999.
12. Souza RD. Development of diamond wire welding device [dissertação]. Florianópolis: Universidade Federal de Santa; 2019.
13. ISO: International Organization for Standardization. Geometrical Product Specifications (GPS) - Surface texture: Profile method - Terms, definitions and surface texture parameters (ISO 4287). Geneve: ISO; 2008.
14. ISO: International Organization for Standardization. Geometrical Product Specifications (GPS) - Surface texture: Profile method - Rules and procedures for the assessment of surface texture (4288). Geneve: ISO; 2008.
15. Weinstein BA, Piermarini GJ. Raman scattering and phonon dispersion in Si and GaP at very high pressure. Phys Rev B. 1975;12(4):1171-86.
16. Liu T, Ge P, Bi W, Gao Y. Subsurface crack damage in silicon wafers induced by resin bonded diamond wire sawing. Mater Sci Semicond Process. 2017;57:147-56.
17. Bifano TG, Dow TA, Scattergood RO. Ductile-regime grinding: a new technology for machining brittle materials. J Eng Ind. 1991;113(2):184-9.
18. Pala U, Kuster F, Wegener K. Characterization of electroplated diamond wires and the resulting workpiece quality in silicon sawing. J Mater Process Technol. 2020;276:1-9.
19. Li HN, Yu TB, Zhu LD, Wang WS. Analytical modeling of grinding-induced subsurface damage in monocrystalline silicon. Mater Des. 2017;130:250-62.
20. Suzuki T, Nishino Y, Yan J. Mechanisms of material removal and subsurface damage in fixed-abrasive diamond wire slicing of single-crystalline silicon. Precis Eng. 2017;50:32-43.
21. Bidiville A, Wasmer K, Kraft R, Ballif C. Diamond wire-sawn silicon wafers - from the lab to the cell production. In: 24th European Photovoltaic Solar Energy Conference. 2009 Sept 21-25; Hamburg, Germany. Proceedings. European Union: European Commission. p. 1-6.
22. Dominich V, Gogotsi Y. Phase transformations in silicon under contact loading. Rev Adv Mater Sci. 2002;3:1-36.
23. Jasinevicius RG, Duduch JG, Montanari L, Pizani PS. Phase transformation and residual stress probed by Raman spectroscopy in diamond-turned single crystal silicon. Proc Inst Mech Eng, B J Eng Manuf. 2008;222(9):1065-73.